IEEE/CSC & ESAS EUROPEAN SUPERCONDUCTIVITY NEWS FORUM (ESNF), No. 11, January 2010
Published in *Journal of Physics Conf. Series* (*SuST*) **234**, 022005 (2010)

Sn concentration gradients in Powder-in-Tube superconductors

M Cantoni[1], C Scheuerlein[2], P-Y Pfirter[1], F de Borman[1], J Rossen[1], G Arnau[2], L Oberli[2] and P Lee[3]

[1] Ecole Polytechnique Fédérale de Lausanne (EPFL), Switzerland
[2] European Organization for Nuclear Research (CERN), Geneva, Switzerland
[3] Applied Superconductivity Center, NMFL, Florida State University, Tallahassee, FL 32310 USA

Corresponding author: Christian.Scheuerlein@cern.ch

Abstract. The Sn concentration gradients across the A15 phase have been studied by Energy Dispersive X-ray Spectroscopy (EDS) measurements. High spatial resolution EDS measurements in the Transmission Electron Microscope reveal a comparatively strong Sn concentration gradient from the periphery towards the centre of individual Nb_3Sn grains.

1. Introduction

The brittle superconducting A15 phase in Nb_3Sn based strands must be formed from the ductile precursor materials by a diffusion heat treatment (HT) at final size. This produces an inhomogeneous Sn concentration within the intermetallic Nb_3Sn compound, which is stable in the approximate compositional range 18-25.5 at.% Sn [1]. A high Sn content and a high chemical homogeneity on a micrometer scale are crucial in order to obtain very high critical current densities (J_c) in Nb_3Sn superconducting strands [2].

The Sn content in Nb_3Sn is commonly measured by Energy Dispersive X-ray Spectroscopy (EDS). The at.% Sn result is an average value over the probed sample volume and, therefore, in inhomogeneous samples the at.% Sn result is a function of the spatial resolution of the EDS experiment. When measured with the spatial resolution of EDS in the Scanning Electron Microscope (SEM/EDS), the concentration gradient across the Nb_3Sn layer of state-of-the-art high J_c strands is in the order of 0.1 at.%Sn/μm. EDS measurements performed in the Transmission Electron Microscope (TEM/EDS) across individual Nb_3Sn filaments in Internal Tin (IT) strands [3] show stronger local Sn concentration gradients than those revealed by EDS/SEM measurements. Here we report Sn concentration gradients on a nanometer scale in the A15 phase of a state-of-the-art PIT strand, as determined by TEM/EDS measurements using electron transparent lamellas prepared by the Focused Ion Beam (FIB) technique.

2. Experimental

The samples analysed are two similar ternary $(Nb\text{-}Ta)_3Sn$/Cu composite strands produced by the PIT process (billets B215 and B179 produced by Shape Metal Innovation (now part of Bruker EAS). Both strands consist of Nb-7.5wt.%Ta precursor tubes that are embedded in a high purity Cu matrix. The Sn precursor is in the form of fine $NbSn_2$ and Sn particles, which are wrapped in a Cu sheath. The B215

strand, which consists of 288 tubes, has a diameter of Ø=1.26 mm and a Cu to non-Cu volume ratio of R=1.22. The PIT B179 strand consists of 192 tubes, has a diameter of Ø=1.02 mm and a Cu to non-Cu volume ratio of R=0.73. The filament diameter in both strands is about 50 μm. After a 84 h-675 °C heat treatment (HT) the non Cu critical current density (J_c) is about 2500 A mm^{-2} and 2400 A mm^{-2} at 12 T and 4.3 K for the B215 and B179 strand, respectively. After a 320 h-625 °C HT of the PIT B215 strand J_c values of about 2700 A mm^{-2} have been measured [4]. Electron transparent lamellas with about 80 nm thickness were prepared by the FIB technique, using a Dual Beam Nova 600 Nanolab system. EDS in TEM was performed in a FEI CM300 FEG-UT TEM/STEM with a Oxford Instruments INCA EDS system and a nominal probe diameter of 1 nm. The EDX in SEM was performed in a FEI XLF30 microscope at 9 kV using an INCAx-act silicon drift detector (SDD).

3. Results

3.1. Nb_3Sn formation

3.1.1. Phase transformations in the Nb-Ta precursor prior to A15 phase formation. The first reaction of the Nb-Ta tubes occurs in the presence of a liquid that is formed in the PIT strand above 415 °C, when Cu_6Sn_5 undergoes a peritectic decomposition [5]. Since there is not enough Cu inside the tubes that could entirely accommodate Sn in a more Cu-rich intermetallic phase, liquid Sn is present in the strand until a significant part of Sn has been incorporated into the Nb-Ta tubes.

A TEM bright field image of the first phase formed at the inner tube periphery is shown in figure 1. Even with the high spatial resolution of the TEM, this region with an approximate composition of 66 at.% Sn, 25 at.% Nb, 8.2 at.% Cu and traces of Ta appears as a single phase and not as a mixture of phases. The formation of a ternary phase has been reported to occur in Internal Tin (IT) strands with high Sn content [6] and it has also been detected in a Tube Type strand [7]. While the elemental composition determined in the PIT strand with TEM/EDS differs somewhat from the compositions reported elsewhere, X-ray diffraction measurements revealed that the crystallographic structure of the presumed Cu-Nb-Sn phase in PIT and IT strands is identical [8].

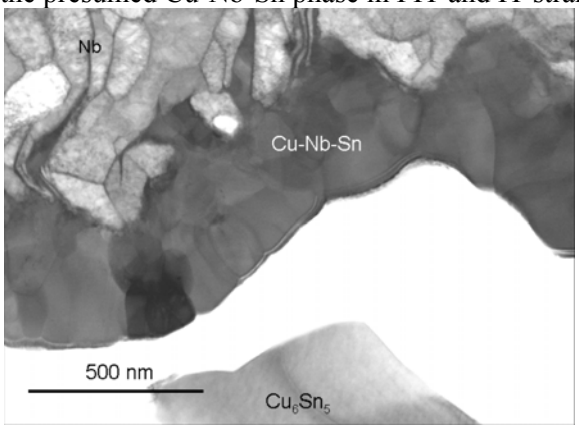

Figure 1: Cu-Nb-Sn ternary phase in the PIT B215 strand after a 480 °C HT. The Cu_6Sn_5 that is detected is re-formed upon cool down to RT.

The $NbSn_2$ phase evolution observed by diffraction measurements during *in-situ* HT with 100 °C/h indicates that $NbSn_2$ formation at the inner surface of the Nb-Ta tubes starts at approximately 550 °C, which is also the approximate temperature at which Cu-Nb-Sn diffraction signals vanish [5].

SEM analysis of PIT [9] and Tube Type [10] fracture samples reveals two distinct Nb_3Sn regions with strongly different Nb_3Sn grain size. It is assumed that the coarse grain Nb_3Sn is formed upon decomposition of Nb_6Sn_5, while the fine grain Nb_3Sn is formed directly by solid state diffusion of Sn into the Nb precursor. First fine grain Nb_3Sn growth occurs in the presence of a Nb_6Sn_5 layer. At 675 °C it needs typically 8 h to transform Nb_6Sn_5 entirely into coarse grain Nb_3Sn and subsequently only fine grain Nb_3Sn is formed [11].

3.1.2. *Nb-Ta precursor grain growth during the reaction HT.* Nb-Ta grain boundaries are potential Nb_3Sn grain nucleation sites. Therefore, the grain boundary density in the Nb-7.5wt.%Ta precursor may influence the Nb_3Sn grain size in the fully reacted strand. The Nb-7.5wt.%Ta grain size in the unreacted PIT B215 strand after a 480 °C HT has been compared with the Nb-7.5wt.%Ta grain size in the diffusion barrier that remains after the full reaction HT (left and right images in figure 2 respectively). It can be seen that the Nb-7.5wt.%Ta grain size after the 675 °C is HT increased with respect to the precursor grain size after the 480 °C HT.

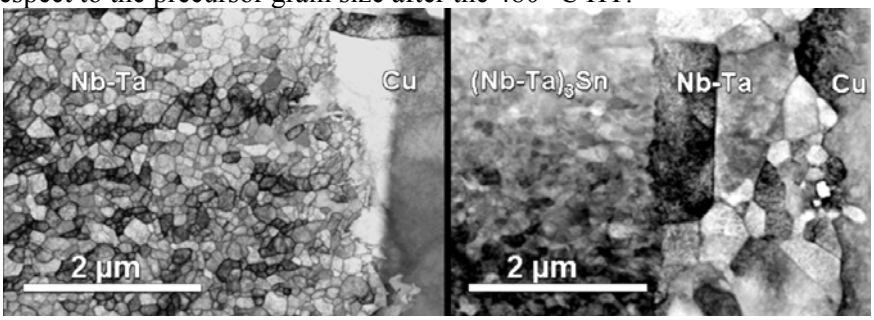

Figure 2: Bright field images of the Nb-7.5wt.%Ta precursor after 480 °C HT (left image) and $(Nb-Ta)_3Sn$ and Nb-Ta in fully reacted PIT strand after 84 h-675 °C HT (right image).

3.2. Concentration gradients

3.2.1. *Sn concentration gradient revealed by SEM/EDS.* A SEM/EDS point scan through the coarse and fine grain region of a PIT B215 subelement after 320 h-620 °C HT is presented in figure 3. The Sn gradient across the fine grain layer is approximately -0.2 at.%/µm, similar to previously reported Sn gradients. A significant Cu gradient is also observed that parallels the decline in Sn composition across the fine grain layer.

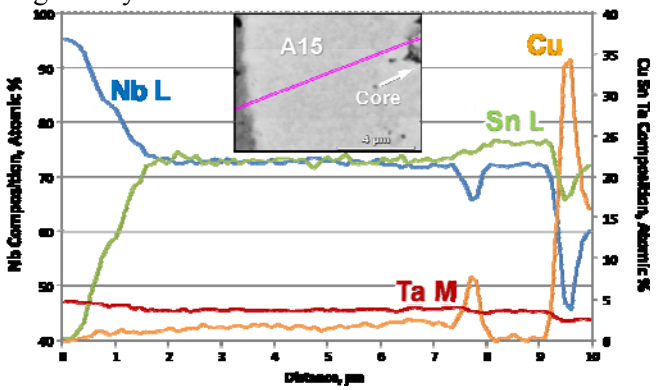

Figure 3: SEM/EDS point scan across the fine and coarse grain A15 layers from the unreacted Nb(Ta) tube to the core for the PIT B215 strand after 320 h-625 °C HT. The Sn composition is approximately 2% higher in the coarse grain region than in the fine grain region.

3.2.2. *Sn concentration gradient revealed by TEM/EDS*. In figure 4 the Sn content variation in the coarse and fine Nb_3Sn regions of the PIT B179 strand is shown. The average Sn content measured by standardless analytical TEM in the fine and coarse grain regions are 22.2 ±0.8 at.%Sn and 24.6±0.2 at.%Sn, respectively (Cu is included in the calculation). In the coarse Nb_3Sn grain region a steady increase of the Sn content towards the fine grain interface is observed. In the fine grain region there is much more scatter (±2at.%) in the measured compositions as it has been observed by SEM/EDS.

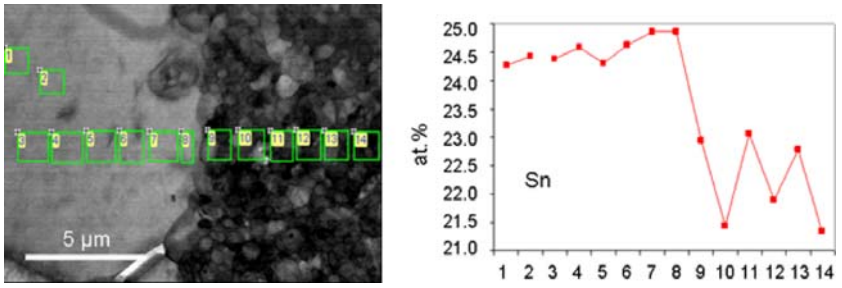

Figure 4: Sn concentration variation across the coarse grain Nb_3Sn (points 1 to 8) and fine grain Nb_3Sn (points 9 to 14). The distance between the measurement points is about one µm.

3.2.3. *Sn concentration gradient on a nanometer scale across individual fine Nb_3Sn grains.* In order to examine the Sn concentration distribution within individual grains TEM/EDS measurements were performed in the fine grain Nb_3Sn region with an estimated spatial resolution of 20 nm. The distance between each data point shown in figure 5 is 40 nm. Measured at.% Sn values spanned the entire Sn composition range expected in Nb_3Sn and the Sn content in the Nb_3Sn grain center tends to be lower than at the grain periphery, although there is considerable scatter in the data. The statistical error in the Sn composition based on the X-ray counts is in the order of 0.5 at.%.

Statistical analysis of the at.% Sn results as a function of the analysis position distance to the grain boundary (see figure 5) suggests a Sn gradient in the order of 0.02 at.%Sn/nm, which is about 10 times the trend across the entire layer. However, this analysis based on an assumed linear dependence is to be considered as a crude estimate. A significantly steeper Sn gradient can not be excluded because the grain boundary distance perpendicular to the cross sectional area could not be taken into account, a Sn gradient on a microscopic scale may be superimposed, and the gradient may not be linear. Further high spatial resolution EDS measurements are needed to determine the Sn gradient inside individual grains with more precision.

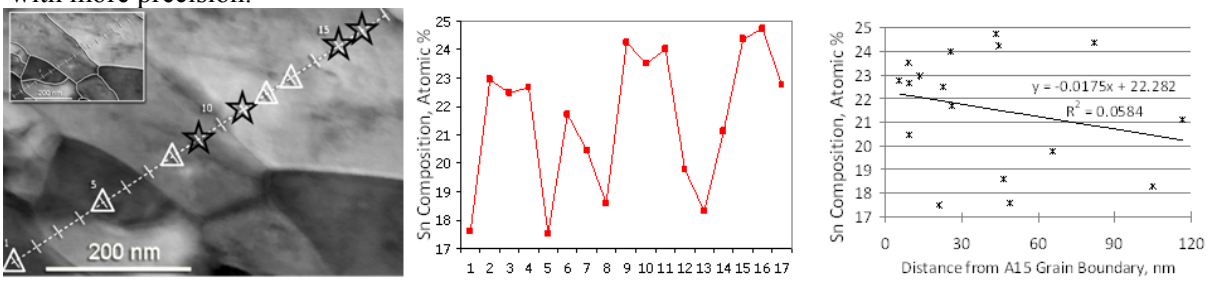

Figure 5: TEM/EDS point scan across four Nb_3Sn grains (identified grain boundaries shown inset top left). Stars indicate locations with compositions greater than or equal to 24 at.%Sn, and triangles indicate locations where Sn was measured below 20 at.%. In the right plot the Sn concentration is presented against the distance to the grain boundary, as measured in the 2-dimensional TEM image. The least square fit calculated trend is approximately 0.02 at.%Sn/nm.

3.2.4. *Composition gradients at the grain boundaries.* The knowledge of the elemental composition of the Nb_3Sn grain boundaries is of interest since it may influence the specific pinning force. A semi-quantitative description of the Cu and Sn concentration gradient across a fine Nb_3Sn grain boundary in PIT B179 is presented in figure 6. The TEM/EDS Cu Lα intensity profile (raw peak intensity) reveals that Cu is concentrated at the grain boundaries.

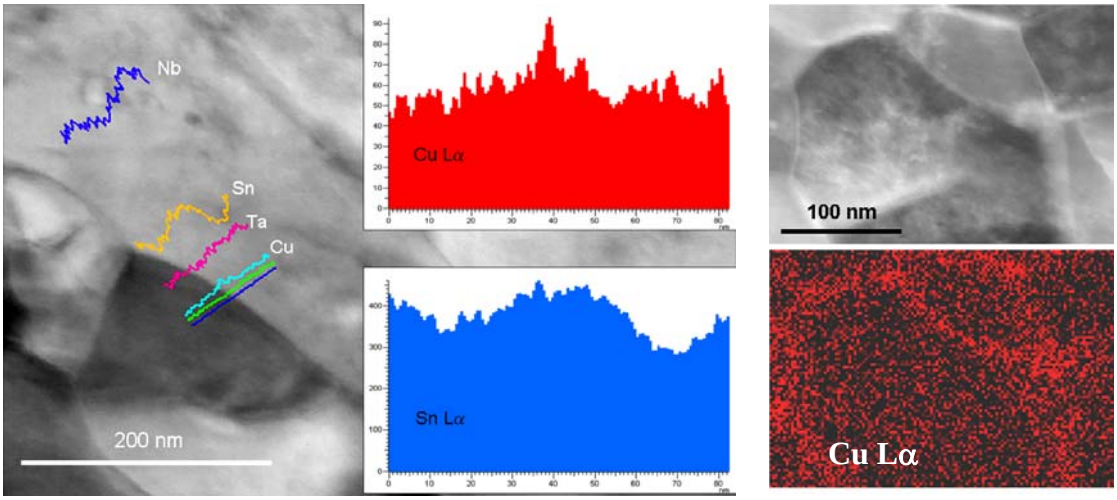

Figure 6: Cu Lα and Sn Lα intensity profiles across a Nb_3Sn grain boundary and Cu chemical map of an individual Nb_3Sn grain (right).

4. Discussion and conclusion

Two types of Sn concentration gradients in PIT strands can be distinguished. SEM/EDS measurements with micrometer resolution reveal a gradient across the equiaxed fine grain Nb_3Sn of about -0.3 at.%Sn/µm from the Sn source outwards to the Nb_3Sn/Nb interface [12], which is similar to the -0.2 at.% Sn/µm observed here.

The high spatial resolution TEM/EDS measurements presented here show that there is a second much steeper gradient from the Nb_3Sn grain periphery to the grain center. These compositional variations extend further into the grains than was observed for bronze processed strands by Auger electron spectroscopy [13]. By TEM/EDS measurements a similarly strong Sn concentration gradient on a nanometer scale has been reported for IT strands [14]. The high concentration gradient across individual grains shows that grain boundary diffusion is dominating the Sn transport through the fine grain Nb_3Sn into the Nb precursor tubes. A small Nb_3Sn grain size is thus not only beneficial for flux pinning (flux pinning force is related to the inverse grain size) but also for obtaining a better chemical Nb_3Sn homogeneity.

The critical temperature (T_c) and critical field (B_{c2}) of homogeneous binary bulk Nb_3Sn vary strongly with Sn content in the range 18-24 at.% Sn, and in this range B_{c2} increases with about 5 T per 1 at.% Sn up to a maximum of about 30 T [15]. Thus, a low-Sn Nb_3Sn grain core may loose superconductivity when a high current is transported in an external field.

Additional TEM/EDS measurements in different Nb_3Sn strand types, using different grains, location and HT, should yield important clues as to how to best optimize HT and precursor composition in the future.

References

[1] J.P. Charlesworth, I. Macphail, P.E. Madsen, J. Mater. Sci. 5, (1970), 580-603
[2] P.J. Lee, D.C. Larbalestier, Cryogenics 48, (2008), 283-292
[3] X. Peng, M.D. Sumption, R. Dhaka, M. Bhatia, M. Tomsic, E. Gregory, E.W. Collings, IEEE Trans. Appl. Supercond. 17(2), (2007), 2668-2671
[4] T. Boutboul1, L. Oberli1, A. den Ouden, D. Pedrini, B. Seeber, G. Volpini, IEEE Trans. Appl. Supercond. 19(3), (2009), 2564-2567
[5] M. Di Michiel, C. Scheuerlein, Supercond. Sci. Technol. 20, (2007) L55-L58
[6] M.T, Naus, P.J. Lee, D.C. Larbalestier, IEEE Trans. Appl. Supercond. 11(1), (2001), 3569-3572

[7] C Scheuerlein, M Di Michiel, L Thilly, F Buta, X Peng, E Gregory, J A Parrell, I Pong, B Bordini, M Cantoni "Phase transformations during the reaction HT of Nb_3Sn strands", submitted manuscript EUCAS6
[8] C. Scheuerlein, M. Di Michiel, G. Arnau, F. Buta, IEEE Trans. Appl. Supercond., (2008)
[9] H. Veringa, P. Hoogendam, A.C.A. van Wees, IEEE Trans. Magn. 19, (1983), 773-776
[10] V.R. Nazareth, M.D. Sumption, X. Peng, E. Gregory, M.J. Tomsic, E.W. Collings, Advances in Cryogenic Engineering 54, (2008)
[11] M. Fischer, "Investigation of the Relationships Between Superconducting Properties and Reaction Conditions in Powder-In-Tube Nb_3Sn Conductors", MSc thesis, University of Wisconsin, (2002)
[12] C.D. Hawes, P.J. Lee, D.C. Larbalestier, Supercond. Sci. Technol. 19, (2006)
[13] M. Suenaga, W. Jansen, Appl. Phys. Lett. 43(8), (1983), 791-793
[14] D. Rodrigues, C.L.H. Thieme, D.G. Pinatti, S. Foner, IEEE Trans. Appl. Supercond., 5(2), (1995), 1607-1610
[15] R. Flükiger, D. Uglietti, C. Senatore, F. Buta, Cryogenics 48, (2008), 293-307